or excess of the delivered dose can cause loss of local tumor control and adverse events in normal tissues. International Commission on Radiation Units and Measurements (ICRU) report 24 [1] and American Association of Physicists in Medicine (AAPM) TG 24 [2] recommended ensuring that the uncertainty in dose distribution calculations be within 3 % of the prescribed dose. The importance of dose calculation accuracy in a radiation treatment planning system (RTPS) for achieving the 3 % objective is described in AAPM TG 65 [3].

The dose calculation accuracy of the RTPS depends on the dose calculation algorithm and the beam model used. Many algorithms have been developed for improving the dose calculation accuracy. However, even in conventional (non-intensity-modulated radiation therapy) fields, a >3 % difference between calculations and measurements can occur, depending on the calculation conditions [4], such as the half-field method, wedge field, and missing tissue [5] within the radiation field. These differences are due to limitations of the algorithms, of the beam model, or both.

The actual radiation dose delivered may differ among institutions even with the same prescribed dose. Thus, it is necessary to understand the differences according to the RTPS and the algorithm(s) used at each institution. Especially in multi-institutional radiation therapy clinical trials, it is important to reduce differences in dose calculation accuracy among the institutions. To minimize this multi-institutional dose variation, the calculation accuracy of the RTPS must be assessed at each institution, by comparison of calculations and measurements. Additionally, third party quality assurance (QA) programs that utilize mailed and on-site dosimetry are used for verification of the linac output and the beam modeling [6].

The calculation accuracy of the RTPS depends on the calculation conditions. In this study, QA for whole breast radiotherapy, which was carried out by many institutions, was performed. AAPM TG 53 [7], European Society for Radiotherapy and Oncology (ESTRO) booklet 7 [8], and International Atomic Energy Agency (IAEA) TRS430 [9] have guidelines for establishing an RTPS-based QA program. However, there is little guidance regarding the establishment of a specialized QA procedure for whole breast radiotherapy before clinical use, and for verifying dose differences among institutions depending on the RTPS, algorithm, and beam model used. We have developed practical procedures for QA of treatment planning systems, based on previous reports [7–9], to verify the dose calculation accuracy at each institution. These procedures were designed to be performed readily at any institution and to facilitate comparisons of results among institutions. In this study, QA for whole breast radiotherapy at seven institutions in Japan was examined, and the dose calculation accuracy of RTPS across these institutions was evaluated with use of the methods devised.

2 Materials and methods

Table 1 lists the linear accelerators and RTPSs used in this study. Linear accelerators with X-ray energies of 4 and 6 MV—Clinac 21EX (Varian Medical Systems, Palo Alto, CA, USA), Clinac iX (Varian Medical Systems, Palo Alto, CA, USA), ONCOR (Siemens AG, Erlangen, Bayern, Germany), and Primus (Siemens AG, Erlangen, Bayern, Germany)—were used. Three types of RTPS were examined: Pinnacle^3 (Phillips Radiation Oncology Systems, Fitchburg, WI, USA), Eclipse (Varian Medical Systems, Palo Alto, CA, USA), and XiO (Elekta CMS, Mayland Heights, MO, USA). The QA program developed for assessment of the dose calculation accuracy of the RTPS is described below.

2.1 Phantom and measurement devices

A Farmer-type ion chamber (PTW30013) and two films [EDR2 radiographic film (Kodak, Tokyo, Japan) and EBT2 radiochromic film (ISP Corporation, Wayne, NJ, USA)] were used as dose detectors. Two types of films were used because not all institutions have appropriate automatic film processors. The uncertainties of measurements by use of EDR2 and EBT2 were the same under the irradiation conditions in this study [10–12].

A solid water-equivalent phantom was used because it is employed by many institutions. Many solid phantoms are commercially available; however, all have similar physical characteristics; specifically, the depth-scaling factor (C_{pl}) [13] and fluence-scaling factor (h_{pl}) [14] are approximately 1.0. In this study, we used the WE211 Tough Water (Kyoto Kagaku, Kyoto, Japan) phantom and RMI457 Solid Water (GAMMEX Inc., Middleton, WI, USA) phantom; the variations of the C_{pl} and h_{pl} of the PTW30013 ionization chamber on these phantoms were within 1 % in our measurements [12, 15].

M. Nozaki
Department of Radiology, Dokkyo Medical University Koshigaya Hospital, 2-1-50 Minami-Koshigaya, Koshigaya City, Saitama 343-8555, Japan

Y. Kagami
Department of Radiology, Showa University Hospital, 1-5-8, Hatanodai, Shinagawa-Ku, Tokyo 142-8555, Japan

T. Nishio
Particle Biology Section, Particle Therapy Division, Research Center for Innovative Oncology, National Cancer Center East, 6-5-1, Kashiwanoha, Kashiwa City, Chiba 277-8577, Japan

Table 1 Materials used in this study

Institution	RTPS	Classified algorithm	Linac
A	Pinnacle^3 ver. 8.0m	SP, CV	Varian 21EX(4X) Varian 21EX(6X)
B	XiO ver. 4.50.03	SP, CV, Clarkson	Varian iX(6X)
C	Eclipse ver. 8.1	SP, PBC	Varian iX(4X)
D	Eclipse ver. 8.1	SP, PBC	Varian 21EX(4X) Varian 21EX(6X)
E	XiO ver. 4.50	SP, CV, Clarkson	Varian 21EX(4X) Siemens ONCOR(6X)
F	Pinnacle^3 ver. 9.0	SP, CV	Siemens ONCOR(6X)
G	XiO ver. 4.50	SP, CV, Clarkson	Varian iX(6X) Siemens PRIMUS(6X)

SP superposition, *CV* convolution, *PBC* pencil-beam convolution, *4X* 4 MV X-ray, *6X* 6 MV X-ray

2.2 Dose calculation

Nine dose calculation algorithms installed in three RTPSs were used for dose calculation in this study, as indicated below.

(1) Pinnacle^3

- Collapsed cone convolution (CCC) [16]
- CCC (with a scatter homogeneous mode) [16]
- Adaptive convolve (AC) [16]
- AC (with a scatter homogeneous mode) [16]

(2) Eclipse

- Anisotropic analytical algorithm (AAA) [17–20]
- Single pencil-beam convolution (PBC) [21, 22]

(3) XiO

- Multigrid superposition (MS) [23, 24]
- Fast Fourier transform convolution (FFC) [23]
- Modified Clarkson sector integration (Clarkson) [25, 26]

The uncertainty factors in the dose calculation accuracy are dependent on the type of algorithm used. The above algorithms were classified into the following four groups: superposition (SP), convolution (CV), pencil-beam convolution (PBC), and Clarkson. SP, CV, and PBC are model-based algorithms that use a convolution method. SP uses a variable dose kernel. CV uses dose kernels of constant shape. In PBC, the lateral scattering is considered to be homogeneous, and the inhomogeneity correction happens only in the longitudinal direction, which is accounted for by use of the equivalent path length converted from the mass attenuation. Clarkson is a measurement-based algorithm. CCC, AC, AAA, and MS were categorized as SP. CCC (with a scatter homogeneous mode), AC (with a scatter homogeneous mode), and FFC were categorized as CV.

The dose calculated by RTPS used the same geometries as those performed by following measurement procedures (see next section). In cases in which dose calculations were determined with use of solid-phantom CT image datasets, the dose calculation accuracy can be affected by the uncertainty in the conversion table of the CT number to relative electron density and by the set-up error in CT acquisition. In this study, we used a virtual phantom to compare only the dose calculation accuracies associated with the dose calculation algorithm and the beam model used at each institution. We created a virtual phantom (30 × 30 × 30 cm–40 × 40 × 40 cm) and assigned it the density of water.

In the RTPS, dose calculations are performed by use of a virtual water phantom; in contrast, dose measurements are performed by use of a water-equivalent solid phantom. Thus, depth and fluence scaling factors are required for correction of the differences between the dose calculation and measurements [12]. However, the measured dose values were not corrected because the effects of C_{pl} and h_{pl} were negligible in our measurements [12, 15]. The dose calculation grid size was set to 2–2.5 mm in this study.

2.3 Measurements

We performed the following procedures to evaluate the dose calculation accuracy of the RTPS. These procedures were designed to be performed readily and rapidly at any institution and to facilitate comparison of the results across institutions.

The absolute dose was determined by use of an ionization chamber that was calibrated at a secondary standard dosimetry laboratory (uncertainty $1\sigma = 1.5$ %). Additionally, for evaluation of the influence of phantom set-up error, the point doses at points 1 mm offset from measurement points in six directions (anterior–posterior, left–right, and superior–inferior) were calculated. The differences between the measurement point dose and the offset point dose were within 1 % for all measurement conditions assessed. Fixed irradiation doses of 100 and 200 monitoring units (MUs) were used for measurements made with the chamber and film, respectively. Point doses calculated by the RTPS were compared with equivalent point dose

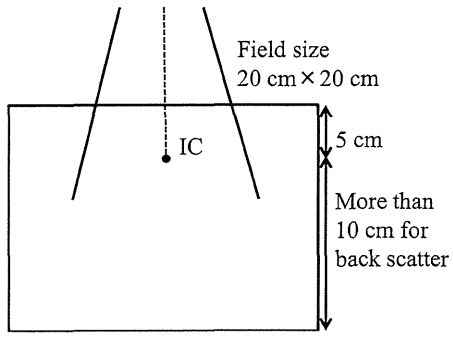

Fig. 1 Simple field measurements with an ionization chamber (gantry angle: 0°, field size: 20 × 20 cm)

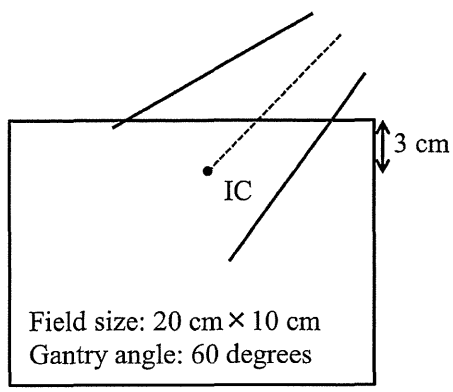

Fig. 2 Oblique field measurements with an ionization chamber (gantry angle: 60°, field size: 20 × 10 cm)

values measured with the chamber. The measurement points were set to the small-dose gradient region, and the differences between the point dose and that to the active volume of the chamber were negligible. The relative errors between the dose calculated with use of each algorithm and the measured dose were calculated.

2.4 Measurements of simple field

Figure 1 shows the geometry of measurements made with an ionization chamber for a simple 20 × 20-cm field (gantry angle of 0°); this was selected because a field of ~20 cm is necessary to cover the whole breast. To assess the output accuracy, including that of the beam model, we measured the absorbed dose using the ionization chamber at the isocenter (IC). The IC point was at 5 cm depth from the surface of the water phantom, with a source-to-surface distance (SSD) of 95 cm.

2.5 Measurements of oblique field

The oblique field technique is used almost exclusively for whole breast radiotherapy. Figure 2 shows the geometry of oblique field technique measurements made with the ionization chamber. The dose at the IC was measured at a gantry angle of 60° and with a field size of 20 × 10 cm and an SSD of 94 cm. This measurement geometry was designed in agreement with common clinical settings of whole breast radiotherapy. The next procedure (missing tissue within the radiation field measurement by use of the ionization chamber) can be performed with the same phantom set-up.

2.6 Measurements of missing tissue within the radiation field

The effects of lack of scatter from the air (missing tissue region) were examined by the measurements shown in Fig. 3a. The dose at a point 5 mm distal from the IC was measured at a gantry angle of 90° and with a field size of 20 × 10 cm and SSDs of 80, 82.5, or 85 cm, according to the phantom size at each institution. In this procedure, the measurements were performed with various SSDs, because the solid water-equivalent phantoms at many institutions (including institutions not participating in this study) can be inserted only into the center of the chamber. The measurement point was determined 5 mm away from the IC to avoid the direct radiation beam that is emitted through the air gap between water-equivalent solid phantoms.

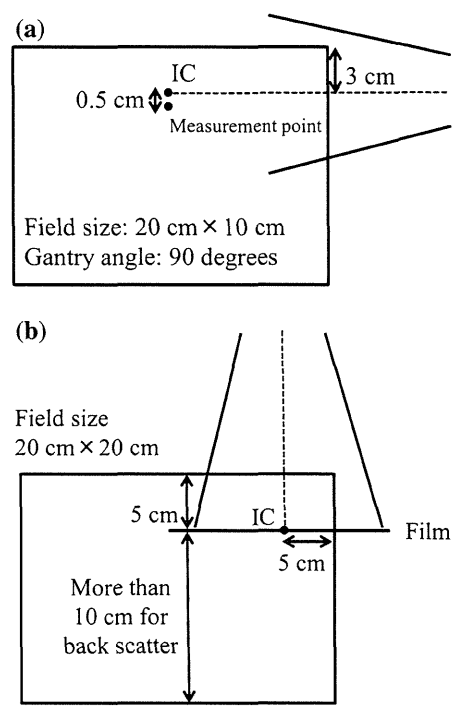

Fig. 3 Measurements for missing tissue conditions with **a** an ionization chamber (gantry angle: 90°, field size: 20 × 10 cm), **b** radiographic or radiochromic film (gantry angle: 0°, field size: 20 × 20 cm)

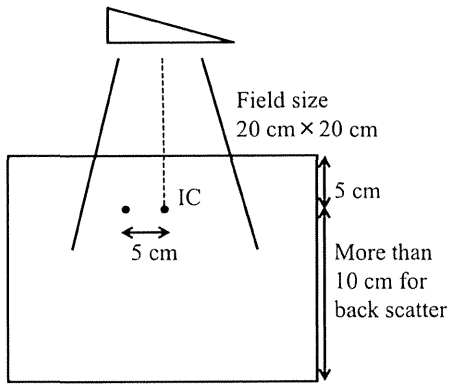

Fig. 4 Wedge field measurements with an ionization chamber (gantry angle: 0°, field size: 20 × 20 cm)

The geometrical arrangements for measurement of the relative dose distribution near the missing tissue region with use of radiographic or radiochromic film are shown in Fig. 3b. Dose profiles were measured at a gantry angle of 0°, a field size of 20 × 20 cm, and a SSD of 95 cm.

2.7 Measurements of wedge field

The wedge field technique is commonly used for whole breast radiotherapy. Figure 4 shows the geometry of measurements with an ionization chamber for the wedge field (a gantry angle of 0°). The absorbed doses at the IC and at a point shifted 5 cm in the lateral direction were measured. The off-axis measurement was performed because the reference point is often set to a location on the off-axis of the beam for whole breast radiotherapy. The chamber was placed in a direction perpendicular to the wedge gradient. The measurements were performed for the physical wedge fields and non-physical wedge (the virtual and dynamic wedge) fields [27–32]. Wedge angles of 15° and 30° were used because these are generally employed for whole breast radiotherapy.

3 Results

The results for each irradiation condition are described below. The results with 4 and 6 MV X-rays did not differ.

3.1 Simple field

The relative errors among the doses calculated by use of each algorithm and the measured dose are shown in Fig. 5. The lower end of the box is the first quartiles, the midline is the second quartiles (median), and the top end is the third quartiles [33]. The individual small circles are outliers [33]. The whiskers are described as far as the highest and lowest values that are not outliers. The same applies to the following figures of the box-and-whisker plot. The means and standard deviations of errors for the SP, CV, PBC, and Clarkson algorithms were 0.5 ± 0.6, 0.3 ± 0.5, 0.1 ± 1.0, and 0.2 ± 0.3 %, respectively. The standard deviation of the relative error calculated with use of the Clarkson algorithm was the smallest.

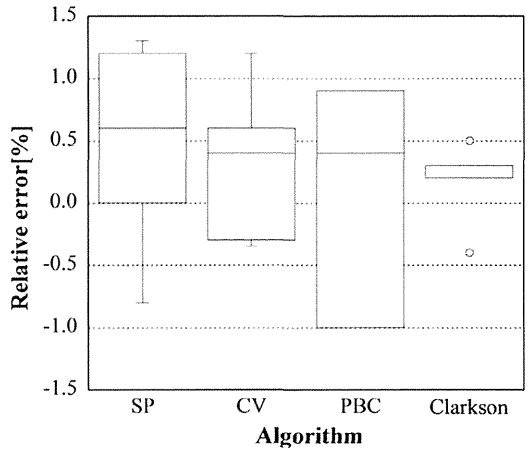

Fig. 5 Relative error between the dose calculated with each algorithm and the dose measured for the simple field (number of samples: SP 11, CV 8, PBC 3, and Clarkson 5). Results are within 2 % agreement. SP corresponds to CCC, AC, AAA, and MS. CV corresponds to CCC (with a scatter homogeneous mode), AC (with a scatter homogeneous mode), and FFC

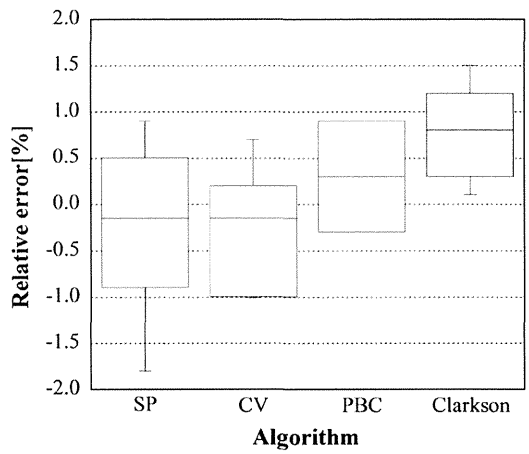

Fig. 6 Oblique field measurements (number of samples: SP, 11; CV, 8; PBC, 3; and Clarkson, 5). Results are within 2 % agreement

3.2 Oblique field

Results for the oblique field measurements are shown in Fig. 6, which also shows the relative error between the doses calculated with use of each algorithm and the measured dose. The means and standard deviations of errors for

the SP, CV, PBC, and Clarkson algorithms were -0.3 ± 0.6, -0.3 ± 0.6, 0.3 ± 0.9, and 0.8 ± 0.6 %, respectively. All calculations and measurements for the oblique field were in good agreement.

3.3 Missing tissue within the radiation field

The results obtained under the missing tissue condition are shown in Figs. 7 and 8. Figure 7 shows the relative error between the doses calculated with use of each algorithm and the measured dose. The means and standard deviations of errors for the SP, CV, PBC, and Clarkson algorithms were -0.1 ± 0.9, -0.6 ± 0.5, 0.3 ± 1.0, and 2.2 ± 0.9 %, respectively. With the exception of the Clarkson algorithm, all relative errors were within 3 %. For the Clarkson algorithm, a maximum 3.4 % difference between calculations and measurements was found. The relative dose profiles calculated with each algorithm and measured with use of film are shown in Fig. 8. The doses were normalized at the IC. The Clarkson algorithm results at the phantom surface were markedly different from those of the other algorithms.

3.4 Wedge field

A comparison of the results of the open, physical wedge, and non-physical wedge fields with use of all algorithms is shown in Fig. 9. The means and standard deviations of the relative errors for the open, physical wedge, and non-physical wedge fields were 0.3 ± 0.6, 0.1 ± 0.5, and 0.8 ± 1.0 %, respectively. The relative errors for the physical wedge fields were within 2 %, which was equivalent to the results for the open fields. For the non-physical wedge field, the standard deviation was higher; a maximum 3.9 % difference between calculations and measurements

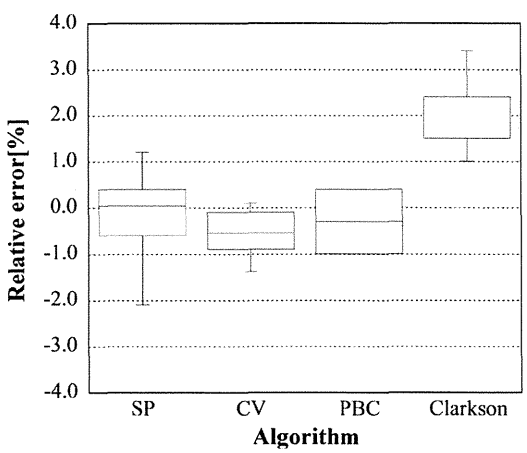

Fig. 7 Relative error between the dose calculated with each algorithm and the dose measured with use of the ionization chamber (number of samples: SP, 11; CV, 8; PBC, 3; and Clarkson, 5). The average and standard deviations of errors for the SP, CV, PBC, and Clarkson algorithms were -0.1 ± 0.9, -0.6 ± 0.5, 0.3 ± 1.0, and 2.2 ± 0.9 %, respectively. For the Clarkson algorithm, a maximum 3.4 % difference between calculations and measurements was observed

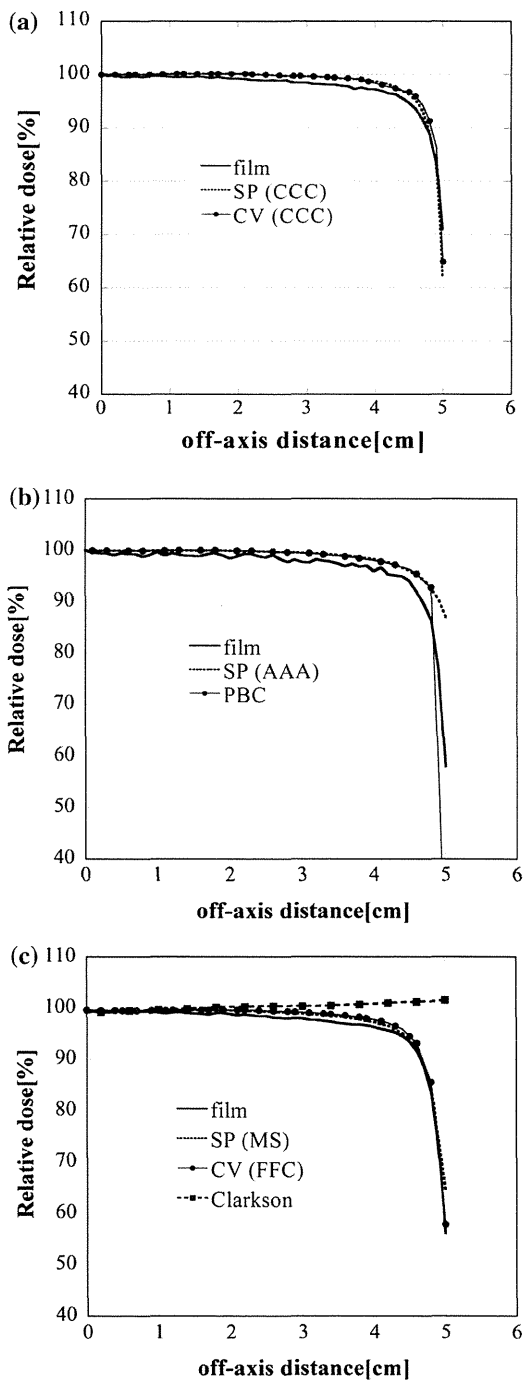

Fig. 8 Dose profile calculated with each algorithm and measured with use of radiographic or radiochromic film. **a** Pinnacle[3] (Institution A, 6X), **b** eclipse (Institution C, 4X), and **c** XiO (Institution B, 6X)

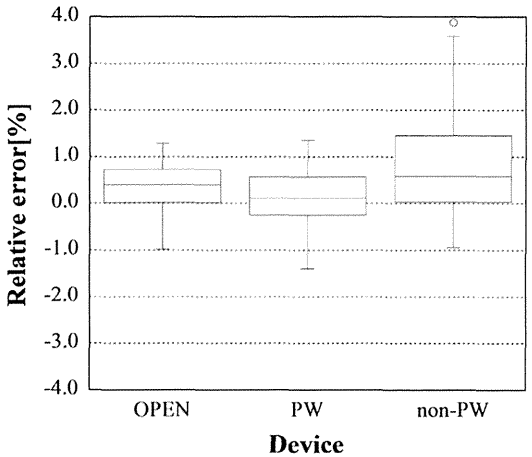

Fig. 9 Comparison of the open, physical wedge, and non-physical wedge conditions (number of samples for each condition: 27). The averages and standard deviations of the relative errors for the open, physical wedge, and non-physical wedge fields were 0.3 ± 0.6, 0.1 ± 0.5, and 0.8 ± 1.0 %, respectively. The uncertainty for the non-physical wedge condition was the greatest

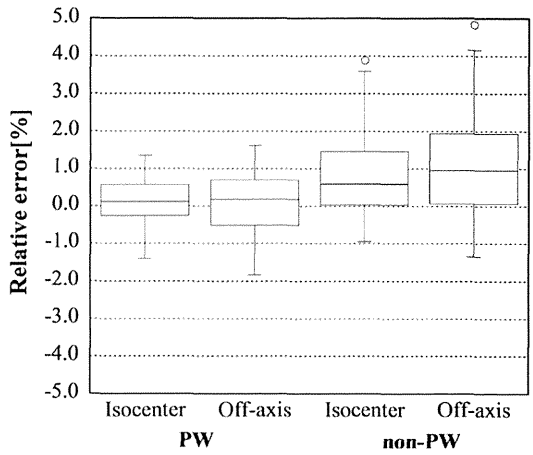

Fig. 10 Comparison of the IC and off-axis conditions with physical wedge and non-physical wedge conditions (number of samples per condition: 27). The averages and standard deviations of the relative error for the physical wedge field at the IC and off-axis were 0.1 ± 0.6 and 0.1 ± 0.9 %, respectively. Likewise, for the non-physical wedge field, the averages and standard deviations at the IC and off-axis were 0.8 ± 1.1 and 1.0 ± 1.4 %, respectively. The uncertainty of the off-axis condition was greater than that of the IC

was found. No difference between the results for 15° and 30° wedges was found.

A comparison of the results obtained at the IC and off-axis with use of physical and non-physical wedge fields, and all algorithms is shown in Fig. 10. The means and standard deviations of the relative errors for the physical wedge field at the IC and off-axis were 0.1 ± 0.6 and 0.1 ± 0.9 %, respectively. Likewise, for the non-physical wedge field, the means and standard deviations at the IC and at the off-axis were 0.8 ± 1.1 and 1.0 ± 1.4 %, respectively. The standard deviation of the off-axis result was greater than that of the IC result. For the non-physical wedge field at the off-axis position, a maximum 4.8 % difference between calculations and measurements was found.

For the results of the non-physical wedge field with use of Pinnacle and Eclipse, all relative errors were within 3 % (mean ± SD %: 0.5 ± 0.7 % and −0.1 ± 1.0 %, respectively). However, >3 % differences between the calculated dose and the measured dose were found in the results with use of XiO (mean ± SD %: 1.3 ± 1.2 %, maximum difference: MS 4.2 %, FFC 3.6 %, and Clarkson 4.8 %).

4 Discussion

For the simple field, the standard deviation of the relative error calculated with use of the Clarkson algorithm was the smallest. In the Clarkson algorithm, the calculations and measurements of a simple field were in good agreement because the measured data were used directly for calculating the dose. The relative errors for all institutions and dose calculation algorithms were within 2 %, which met the recommended criteria specified in a previous report [8]. This indicates that the linac output and the beam model used for the simple field in RTPS at each institution were accurate.

All calculations and measurements for the oblique field were in good agreement. The dose calculations of the oblique field in the homogeneous phantom by use of model-based algorithms were generally accurate [16–24]. For the Clarkson method, a measurement-based algorithm, the dose calculation accuracy was lower than that with use of model-based algorithms because this method does not reproduce the scattered radiation inside the phantom accurately [5, 26]. In this study, all dose calculation algorithms, including Clarkson, demonstrated adequate accuracy. Thus, the dose calculation accuracy with use of SP, CV, PBC, or Clarkson was affected only negligibly by the oblique incidence.

For the missing tissue condition, the Clarkson algorithm results at the phantom surface were markedly different from those of the other algorithms. This dose reduction near the phantom surface is a result of the reduction in scattered photons at the missing tissue region within the radiation field, and the dose reductions near the phantom surface were reproduced with the exception of the Clarkson algorithm. However, a difference between the dose profile near the phantom surface calculated by AAA and PBC was found. This difference might be due to the differences in the resolution of beam model between AAA and PBC. On

the other hand, the Clarkson algorithm does not take into consideration the reduction in scattered radiation [26]. As a result, the calculated dose on the phantom surface is higher than the actual measurement. These relative errors resulting from the characteristics of the calculation algorithms should be taken into consideration during treatment planning and dose evaluation. Furthermore, the reference point for the prescribed dose should not be assigned to a point near the patient's body surface because the surface dose reduction is not assessed accurately by the Clarkson algorithm.

For the non-physical wedge field, the standard deviation was higher than that of the open and physical wedge fields. Additionally, >3 % differences between the calculated dose and the measured dose were found in the results with use of XiO. Generally, the RTPS parameters (e.g., the energy spectrum) should be adjusted by use of measurement data corresponding to simple fields, including percentage depth dose, off-axis ratio, and an output factor for beam modeling [34]. However, the non-physical wedge field is constructed by use of the movement of the jaws at a variable dose rate [27–32]. The parameters that can be adjusted in the non-physical wedge field are dependent on the type of RTPS (including version) used. Thus, generating accurate beam models for the non-physical wedge field is difficult. Moreover, assessing the accuracy of the beam model used at each institution and understanding the characteristics of the dose calculation algorithm are important. Additionally, the accuracy of the RTPS should be improved as much as possible, and the clinical application of the non-physical wedge field should be evaluated.

5 Conclusions

In radiation therapy, the actual prescribed irradiation dose is expected to be similar across institutions. We established a QA procedure to standardize the whole breast radiotherapy irradiation dose used at multiple institutions. Our findings showed that the dose calculation accuracy differs among institutions because it is dependent on the dose calculation algorithm and beam modeling used. For minimizing this dose variation, it is necessary to assess the beam model accuracy and to understand the characteristics of the dose calculation algorithm used at each institution. Additionally, third party QA programs can be used for assessment of the linac output and of beam modeling.

The QA procedures used in this study will facilitate assessment of the accuracy of the dose calculation algorithm and beam model before clinical use for whole breast radiotherapy. In the clinical situation, the irradiation conditions of whole breast radiotherapy are significantly different from the conditions with use of the solid water-equivalent phantom in this study. Further investigations should evaluate the dose calculation accuracy of the RTPS in heterogeneous media, as well as the influence of the reference point position, by use of a breast-shaped phantom.

Acknowledgments This study was performed by the Medical Physics Working Group in the Radiation Therapy Study Group of the Japan Clinical Oncology Group. It was supported in part by the National Cancer Center Research and Development Fund (23-A-21).

Conflict of interest The authors declare that they have no conflict of interest.

References

1. ICRU. Determination of absorbed dose in a patient irradiated by beams of X or gamma rays in radiotherapy procedures. ICRU Report 24. Washington (DC): ICRU; 1976. 67 p.
2. AAPM. Physical aspects of quality assurance in radiation therapy. AAPM report no. 13. New York: American Institute of Physics; 1984.
3. AAPM. Tissue inhomogeneity corrections for megavoltage photon beams. AAPM report no. 85. 2004.
4. ESTRO. Monitor unit calculation for high energy photon beams—practical examples. ESTRO booklet no. 6. 2001.
5. Stern RL, Heaton R, Fraser MW. Verification of monitor unit calculations for non-IMRT clinical radiotherapy report of AAPM Task Group 114. Med Phys. 2011;38(1):504–30.
6. Molineu A, Followill DS, Balter PA, et al. Design and implementation of an anthropomorphic quality assurance phantom for intensity-modulated radiation therapy for the radiation therapy oncology group. Int J Radiat Oncol Biol Phys. 2005;63(2):577–83.
7. Fraass B, Doppke K, Hunt M, et al. American Association of Physicists in Medicine Radiation Therapy Committee Task Group 53: quality assurance for clinical radiotherapy treatment planning. Med Phys. 1998;25(10):1773–829.
8. ESTRO. Quality assurance of treatment planning systems practical examples for non-IMRT photon beams. ESTRO booklet no. 7. 2004.
9. IAEA. Commissioning and quality assurance of computerized planning systems for radiation treatment of cancer. IAEA Technical report series (TRS) no. 430. 2004.
10. Shi C, Papanikolaou N, Yan Y, et al. Analysis of the sources of uncertainty for EDR2 film-based IMRT quality assurance. J Appl Clin Med Phys. 2006;7:1–8.
11. van Battum LJ, Hoffmans D, Piersma H, et al. Accurate dosimetry with GafChromic EBT film of a 6 MV photon beam in water: what level is achievable? Med Phys. 2008;35:704–16.
12. Japan Society of Medical Physics (JSMP). Research report of the dosimetric verification of IMRT. JJMP. 2010; 30(6):1–210 (in Japanese).
13. IAEA. The use of plane-parallel ionization chambers in high-energy electron and photon beams. An international code of practice for dosimetry. IAEA TRS no. 381. 1995.
14. IAEA. Absorbed dose determination in external beam radiotherapy: an international code of practice for dosimetry based on standards of absorbed dose to water. IAEA TRS no. 398. 2004.
15. Fujita Y, Tohyama N, Myojoyama A, et al. Depth scaling of solid phantom for intensity modulated radiotherapy beams. J Radiat Res. 2010;51(6):707–13.

16. Ahnesjo A. Collapsed cone convolution of radiant energy for photon dose calculation in heterogeneous media. Med Phys. 1989;16(4):577–92.
17. Esch AV, Tilikainen L, Pyykkonen J, et al. Testing of the analytical anisotropic algorithm for photon dose calculation. Med Phys. 2006;33:4130–48.
18. Ulmer W, Harder D. A triple Gaussian pencil beam model for photon beam treatment planning. Z Med Phys. 1995;5:25–30.
19. Ulmer W, Harder D. Applications of a triple Gaussian pencil beam model for photon beam treatment planning. Z Med Phys. 1996;6:68–74.
20. VARiAN medical systems. Eclipse algorithms reference guide. 2006; I:2–3—I:2–25.
21. Storchi P, Woudstra E. Calculation of the absorbed dose distribution due to irregularly shaped photon beams using pencil-beam kernels derived from basic beam data. Phys Med Biol. 1996;41(4):637–56.
22. Storchi PR, van Battum LJ, Woudstra E. Calculation of a pencil-beam kernel from measured photon beam data. Phys Med Biol. 1999;44(12):2917–28.
23. Miften M, Wiesmeyer M, Monthofer S, et al. Implementation of FFT convolution and multigrid superposition models in the FOCUS RTP system. Phys Med Biol. 2000;45(4):817–33.
24. Miften M, Wiesmeyer M, Kapur A, et al. Comparison of RTP dose distributions in heterogeneous phantoms with the BEAM Monte Carlo simulation system. J Appl Clin Med Phys. 2001;2(1):21–31.
25. Clarkson JR. A note on depth doses in fields of irregular shape. Br J Radiol. 1941;14:265–8.
26. Khan FM. The physics of radiation therapy third edition. Chapter 9: Dose distribution and scatter analysis. Philadelphia: Lippingcott Williams & Wilkins, 2003. pp. 159–177.
27. Bidmead AM, Garton AJ, Childs PJ. Beam data measurements for dynamic wedges on Varian 600C (6-MV) and 2100C (6- and 18-MV) linear accelerators. Phys Med Biol. 1995;40(3):393–411.
28. Klein EE, Low DA, Meigooni AS, et al. Dosimetry and clinical implantation of dynamic wedge. Int J Radiat Oncol Biol Phys. 1995;31(3):583–92.
29. Liu C, Zhu TC, Palta JR. Characterizing output for dynamic wedges. Med Phys. 1996;23(7):1213–8.
30. Liu HH, McCullough EC, Mackie TR. Calculating dose distributions and wedge factors for photon treatment fields with dynamic wedges based on a convolution/superposition method. Med Phys. 1998;25(1):56–63.
31. Weber L, Ahnesjo A, Nilsson P. Verification and implementation of dynamic wedge calculations in a treatment planning system based on a dose-to-energy-fluence formalism. Med Phys. 1996;23(3):307–16.
32. Thomas SJ, Foster KR. Radiotherapy treatment planning with dynamic wedges—an algorithm for generating wedge factors and beam data. Phys Med Biol. 1995;40(9):1421–33.
33. Michael F, David CH, Boris I. Some implementations of the boxplot. Am Stat. 1989;43(1):50–4.
34. Ezzell GA, Galvin JM, Low D, et al. Guidance document on delivery, treatment planning, and clinical implementation of IMRT: report of the IMRT subcommittee of the AAPM Radiation Therapy Committee. Med Phys. 2003;30(8):2089–115.

Journal of Radiation Research, 2014, 55, 816–822
doi: 10.1093/jrr/rrt230 Advance Access Publication 13 May 2014

Short Communication

Enhanced radiobiological effects at the distal end of a clinical proton beam: *in vitro* study

Yoshitaka MATSUMOTO[1,*], Taeko MATSUURA[2,3], Mami WADA[1], Yusuke EGASHIRA[3], Teiji NISHIO[3] and Yoshiya FURUSAWA[1]

[1]Research Center for Charged Particle Therapy, National Institute of Radiological Sciences, 4-9-1 Anagawa, Inage-ku, Chiba 263-8555, Japan
[2]Advanced Medical Sciences, Graduate School of Medicine, Hokkaido University, 15-7 Kita, Kita-ku, Sapporo, Hokkaido, 060-8638, Japan
[3]Research Center for Innovative Oncology, National Cancer Center Hospital East, 6-5-1 Kashiwanoha, Kashiwa, Chiba 277-8577, Japan
*Corresponding author. Next Generation Medical Physics Research Program, Research Center for Charged Particle Therapy, National Institute of Radiological Sciences, 4-9-1, Anagawa, Inage-ku, Chiba 263-8555, Japan. Tel: +81-43-206-3482; Fax: +81-43-206-4149; Email: y_matsu@nirs.go.jp

(Received 14 July 2013; revised 13 December 2013; accepted 28 December 2013)

In the clinic, the relative biological effectiveness (RBE) value of 1.1 has usually been used in relation to the whole depth of the spread-out Bragg-peak (SOBP) of proton beams. The aim of this study was to confirm the actual biological effect in the SOBP at the very distal end of clinical proton beams using an *in vitro* cell system. A human salivary gland tumor cell line, HSG, was irradiated with clinical proton beams (accelerated by 190 MeV/u) and examined at different depths in the distal part and the center of the SOBP. Surviving fractions were analyzed with the colony formation assay. Cell survival curves and the survival parameters were obtained by fitting with the linear–quadratic (LQ) model. The RBE at each depth of the proton SOBP compared with that for X-rays was calculated by the biological equivalent dose, and the biological dose distribution was calculated from the RBE and the absorbed dose at each position. Although the physical dose distribution was flat in the SOBP, the RBE values calculated by the equivalent dose were significantly higher (up to 1.56 times) at the distal end than at the center of the SOBP. Additionally, the range of the isoeffective dose was extended beyond the range of the SOBP (up to 4.1 mm). From a clinical point of view, this may cause unexpected side effects to normal tissues at the distal position of the beam. It is important that the beam design and treatment planning take into consideration the biological dose distribution.

Keywords: proton beam; biological effectiveness; distal end; cell survival; spread-out Bragg-peak

INTRODUCTION

Proton beam therapy is considered a new yet well-established modality of treatment for cancer and non-cancer diseases around the world [1–4]. The number of proton therapy facilities in the world, especially in Japan, has increased, and it has doubled within the last 10 years [5, 6]. More than 60 000 patients have been treated with proton beams, and high control rates for localized tumors have been reported [1–4, 7]. In recent years, advanced proton therapy [e.g. intensity-modulated proton therapy (IMPT)] has been adapted for irregularly shaped tumors, and the effect is beginning to examined by physical fundamental research [5, 6, 8, 9]. The International Commission on Radiation Units and Measurements (ICRU) recommends defining proton therapy doses as the product of the relative biological effectiveness (RBE) and the physical dose of the proton, with its unit as Gy [11, 12]. Recently, most clinical proton facilities have used a constant RBE value of 1.1, meaning that protons are assumed to be 10% more effective than X-rays or gamma-rays at all positions along the depth–dose distribution [11–14]. The RBE weighting factor of 1.1 was a consequence of several reviews of the available radiobiological data at those instances [12, 15, 16], with most studies determining the RBE in the center of SOBP. However, there is a

general consensus that the RBE of protons depends on the position along the penetration depth [17–20]. Recent physical simulation results suggest the RBE is not constant and that it depends on many factors such as beam energy, dose, depth, radiation quality, and track structure [12, 21–23]. Additionally, modeling studies suggest that there are significant differences between the biologically weighted dose and the absorbed dose distributions for both tumor and normal tissues (using a theoretical variable RBE value to calculate an RBE-weighted proton treatment plan [24–26]). Although many studies have measured the RBE of protons, the experimental conditions were very diverse, with respect to differences in beam energy, position along the depth–dose distribution, method of calculating RBE, and cells used.

In this study, we have determined the RBE at various depths within the SOBP of clinical proton beams with an incident energy of 190 MeV, and have assessed the biological equivalent dose distribution of proton beams. We have also determined the shift of the distal edge of the biological dose compared with the isoeffective dose.

MATERIALS AND METHODS

Cell cultures

A human salivary gland tumor cell line, HSG (JCRB1070: HSGc-C5), was used in this study. The HSG is a standard reference cell line for the intercomparison of RBE among carbon and proton facilities in Japan, and is also used in other countries, including Germany and Korea [25, 27–32]. Cells were cultured in Eagle's MEM supplemented with 10% fetal bovine serum (FBS) and antibiotics (100 U/ml penicillin and 100 µg/ml streptomycin) and incubated under a humidified atmosphere with 5% CO_2 and 95% air at 37°C. Subcultured cells were harvested and seeded in a chamber slide flask (Lab-Tech SlideFlask 170920, Nunc) at ~1.5–2.0×10^5 cells/flask with 3 ml of the medium, and incubated in the incubator for 2 d prior to the experiment. The flasks were fully filled with additional medium on the same day or 1 d before the experiment.

Irradiation

Horizontal proton beams were accelerated up to 190 MeV by an Azimuthally Varying Field (AVF) cyclotron at the NCCHE (National Cancer Center Hospital East) [31]. In this experiment, we used the nozzle designed for the dual-ring scattering method [24] to obtain a flat dose profile and stable dose intensity over the target area. The proton beam was scattered using two thin scatters on the beam line. These scatters made it possible to obtain a flat dose profile over the target area (±2.5% over a 2×5 cm^2 field). The beam was then cut off using collimators. The profile to the center position of the physical depth–dose distribution of the 5 cm-SOBP (from 125 to 175 mmH_2O) was less than ±7.2% (Fig. 1A).

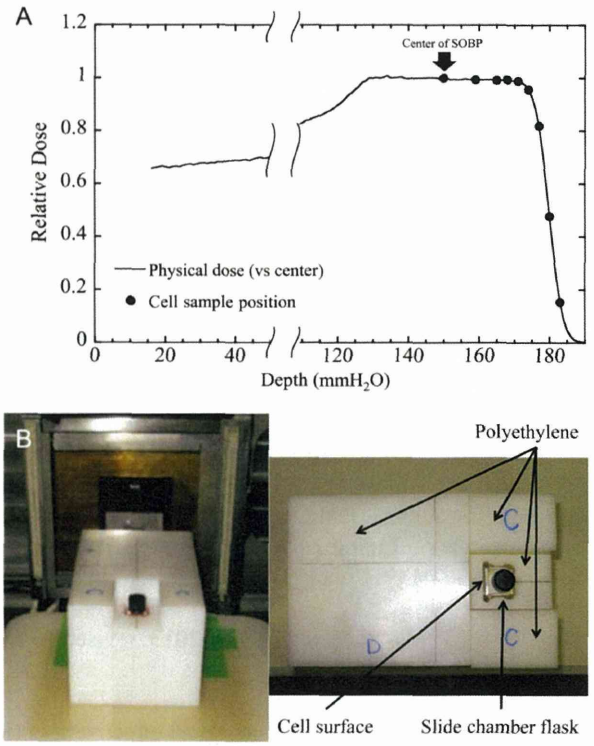

Fig. 1. (**A**) Depth–dose distribution of the spread-out Bragg-peak (SOBP) of the 190 MeV proton beam used in the present experiment. The depth–dose measurement was performed in a water phantom. The closed dots show the irradiation position of each cell sample (150, 159, 165, 168, 171, 174, 177, 180 and 183 mmH_2O). (**B**) The cell sample flask was placed in a specially designed polyethylene block (0.98 g/cm^3) containing a space to hold it. The thickness of the polyethylene block in front of the flask was chosen to locate the cells at the adequate depth of the spread-out Bragg-peak (SOBP) beam.

HSG cells on the bottom of the chamber slide flasks were set in a specially designed polyethylene block (0.98 g/cm^3), and the cell surface was placed at the isocenter of the gantry (Fig. 1B). The depths (at 150, 159, 165, 168, 171, 174, 177, 180 and 183 mmH_2O) in the beam were selected using polyethylene blocks of various thicknesses placed immediately upstream of the cells. The measurement of the dose and dose-rate was conducted with PTW Markus Chamber (Type 23343; PTW, Freiburg, Germany) and an electrometer (FLUKE35040; Fluke Biomedical, Cleveland, OH). Subsequently, GafChromic EBT film (International Specialty Products, Wayne, NJ) was used for verification. We also measured the dose per monitor unit at the center of the SOBP, and used the average value calculated from at least three measurements on each experimental day. The dose rate was ~2–3 Gy/min at each depth.

As for the reference radiation beam, 6 MV X-rays generated by a linac therapy machine at the NIRS (National Institute of Radiological Sciences) were used. The irradiation

doses were measured with the thimble chamber according to the protocol of Japanese Standard Dosimetry 01 [33] for X-rays. The dose rate was ~3 Gy/min. All irradiation was carried out at room temperature, and all experiments were repeated at least three times. X-ray experiments were performed as additional experiments at NIRS, because the treatment schedule of NCCHE was crowded. However, X-ray experiments were performed under the same conditions (i.e. lot and passage number of cells, sample preparation, and assay environment) as the proton beam experiment. We suspect the error caused by carrying out the proton and X-ray beam experiments on different day is not significant.

In vitro clonogenic cell survival assay

After irradiation, cells were rinsed twice with PBS, once with 0.05% trypsin solution containing 1 mM EDTA and maintained at 37°C for 3–5 min. The cells were harvested and their number counted using a particle analyzer (Coulter Z1). The cells were then adequately diluted with the medium and seeded in three 60-mm dishes at densities from 100–50 000 cells per dish to yield ~100 colonies per dish, depending on the radiation dose and the linear energy transfer (LET). Three colony dishes were made per dose within one experiment. Samples were incubated for 13 d, and then the colonies were rinsed with PBS, fixed with 10% formalin solution for 10 min, washed with tap water, stained with 1% methylene blue solution, and dried in air. Colonies consisting of > 50 cells were counted under a stereomicroscope as the number of viable cells.

Analysis of the survival curve

Dose–response curves of HSG cells were fitted by a linear–quadratic equation. The parameters α and β were calculated by logistic curve-fitting using the weighted least-squares method (Kaleida Graph 4.1.4, Hulinks). The α and β values were used to calculate the biological equivalent doses, D_{10} and D_{60} values, the dose required for the cell survival to be 10 and 60%, respectively. D_{60} corresponds approximately to the survival fraction for 2 Gy X-rays for this cell type (Fig. 2 and Table 1). The RBE_{10} and RBE_{60} values of the proton beam were calculated as the ratio of the D_{10} and D_{60} values to that of 6 MV X-rays.

Statistical analysis

Data are presented as the mean ± standard error (SE) of at least three independent experiments. To examine the differences between averages of values, a two-sided Student's *t*-test was used when the variances of two groups could be assumed to be equal. A *P*-value < 0.05 was considered statistically significant.

RESULTS

Survival of HSG cells exposed to proton beams at several depths

The dose–response curves for HSG cells to X-rays and proton beam SOBPs at each depth are shown in Fig. 2. The D_{10} and D_{60} values were calculated from the α and β values (Table 1). The SOBP beam at the center (150 mmH_2O) killed HSG cells more efficiently than the X-rays (Fig. 2A), and the effects increased gently from 159 to 168 mmH_2O in the SOBP beam (Fig. 2B–D, Table 1) compared with at the center. However, the cytotoxic effects increased dramatically after 171 mmH_2O, and the survival curves were similar to each other at higher values (Fig. 2E–I, Table 1).

For HSG cells, the α values of protons tended to be larger than for that of linac X-rays, while the β values tended to remain stable. The α/β ratio was 6.8 Gy for X-rays. The value once decreased in the 150–168 mmH_2O region (4–6 Gy), increased a little (7–9 Gy) in the 171–177 mmH_2O region, and increased suddenly (approximately 15 Gy) at 180 and 183 mmH_2O (Table 1).

Change of RBE in SOBP

The RBE_{10} and RBE_{60} to the depth in SOBP that correspond to D_{10} and D_{60} are shown in Fig. 3. D_{10} values are commonly used to compare the cytotoxic effects of radiation types. HSG cells presented RBE_{10} values of 1.24 and RBE_{60} values of 1.20 at the center of proton SOBP. The RBE values showed a tendency to increase with the depth of proton SOBP, and the maximum value was 1.86 at 180 mmH_2O. These values mean that the proton SOBP beam showed ~50% stronger cytotoxic effects at the distal position compared with at the center of the SOBP.

The depth–dose distributions are shown in Fig. 4. The normalized absorbed dose refers to the relative physical dose normalized to the center of the SOBP. A generic RBE value of 1.1 for protons is used in clinical situations, and an Isoeffective dose $D_{IsoE} = D \times 1.1$ is proposed [11]. The profile of the biological effective dose in this paper can be calculated from the RBE_{10} or RBE_{60} at each depth multiplied by the physical dose at that depth. The biological effective doses at the center of the SOBP were slightly higher than the isoeffective dose (Fig. 4). The values of biological effective doses were not significantly changed between 150 and 168 mmH_2O, significantly increased at a depth of 171 to 177 mmH_2O, then decreased with decrease of physical dose, however the biological effective dose was still higher than the isoeffective dose at 180 and 183 mmH_2O. Additionally, in the current study, the distal edge of the biological dose was extended ~3.6 mm for RBE_{10} and 4.1 mm for RBE_{60} from the edge of SOBP obtained by the isoeffective dose.

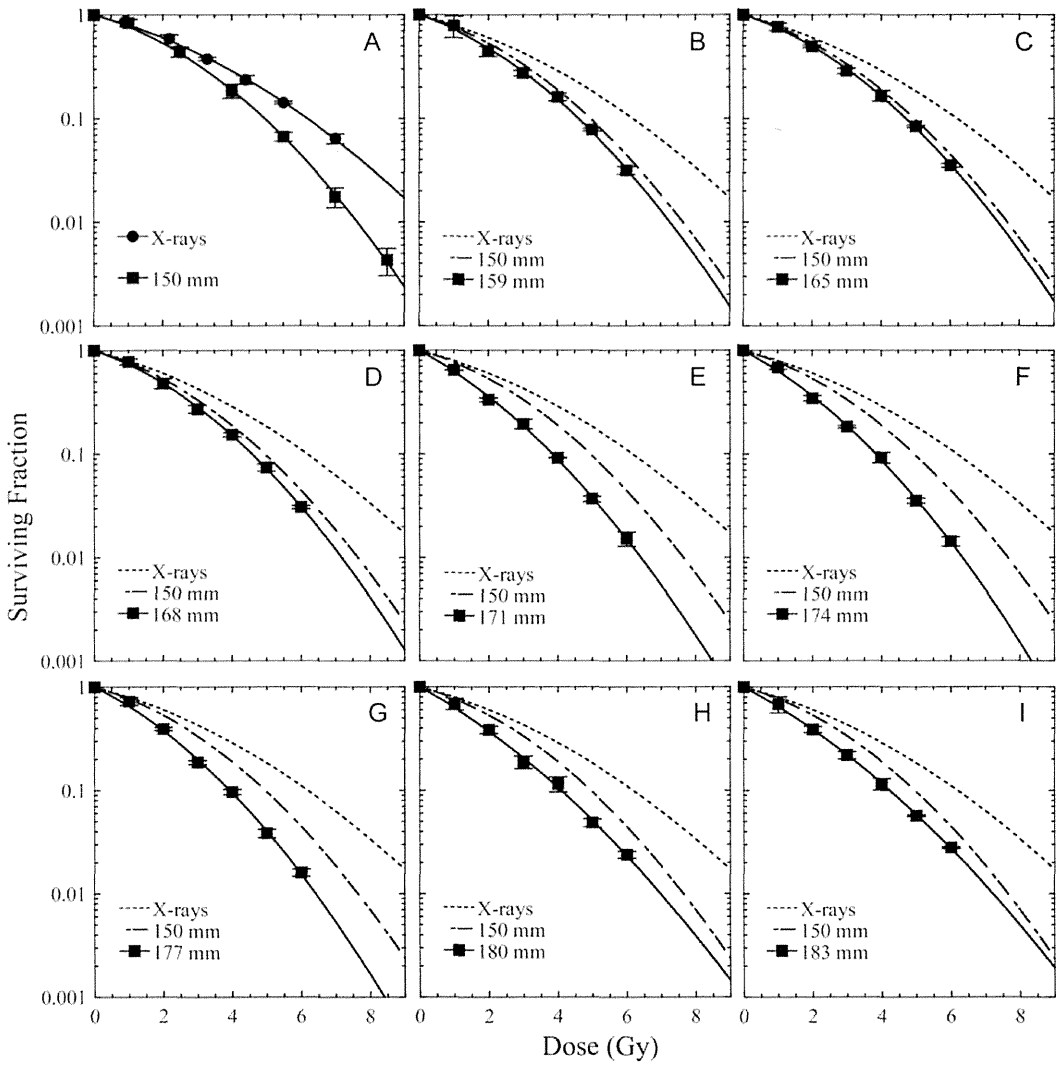

Fig. 2. Dose–response curves of HSG cells irradiated with X-rays (closed circles) or at each depth of the proton SOBP (closed squares). All datapoints were fitted by the linear–quadratic (LQ) model. The symbols and bars are the mean and standard error (SE) obtained from at least three independent experiments. The symbols and bars of the reference X-rays data and the center of the SOBP as a reference data are indicated only in Fig. 3A, and the fitted curves (dotted line for X-rays and dashed line for center of the SOBP) for the various positions are indicated in Fig. 3B–I. Horizontal axis, Dose (Gy) means the physical absorbed dose of X-rays and protons at each depth.

DISCUSSION

Here, we have reported the RBE dependence of the biological depth–dose distribution at several depth positions of 190 MeV proton beams accelerated by a cyclotron and in the SOBP generated by the dual-ring scattering method. A generic RBE of 1.1 is recommended for the whole region of proton SOBPs for all clinically relevant applications worldwide [11, 13, 14, 34]. Therefore, all clinical applications are conducted at that RBE value, and the flat adsorbed depth–dose distribution is used in the therapies. However, some studies have demonstrated an increase in the RBE at the end of the proton SOBP using physical simulations [22, 23] and analysis of published biological results [11]. Wilkens *et al.* reported that the RBE of the distal region of a SOBP increased to 1.18–1.60 depending on the fraction size of 1–8 Gy per fraction in the case of 160-MeV protons [22]. In the present study, the RBE values varied with depth and were higher at the distal-end of the SOBP for 190 MeV clinical protons. This result suggests that it is necessary to set the absorbed depth–dose distribution according to the differences in the biological effect. The RBE of protons could depend on the fraction size. The conventional fractionation scheme of proton therapy is ~2 GyE (generic RBE 1.1 × physical dose) per fraction [35]. The effective doses of the proton SOBP that correspond to 2 Gy X-rays were calculated

Table 1. The surviving parameters and biological equivalent dose for HSG cells in a 190 MeV clinical proton beam with a 5-cm spread-out Bragg-peak (SOBP) at each depth compared with the center

	X-rays	Proton									
		Depth in H_2O (mm)									
		150	159	165	168	171	174	177	180	183
α (Gy^{-1})	0.19 ± 0.03[a]	0.22 ± 0.07	0.28 ± 0.07	0.25 ± 0.04	0.26 ± 0.03	0.42 ± 0.01	0.41 ± 0.04	0.38 ± 0.03	0.44 ± 0.06	0.42 ± 0.07
β (Gy^{-2})	0.03 ± 0.01	0.05 ± 0.01	0.05 ± 0.01	0.05 ± 0.01	0.05 ± 0.01	0.05 ± 0.01	0.05 ± 0.01	0.05 ± 0.01	0.03 ± 0.01	0.03 ± 0.01
α/β (Gy)	6.82 ± 2.83	4.40 ± 0.85	5.85 ± 2.60	5.08 ± 1.25	5.00 ± 1.01	9.12 ± 0.91	8.44 ± 2.04	7.34 ± 1.49	14.9 ± 5.56	15.6 ± 7.15
SF_2	0.60 ± 0.01	0.53 ± 0.01	0.48 ± 0.03	0.49 ± 0.02	0.48 ± 0.01	0.36 ± 0.01	0.36 ± 0.01	0.38 ± 0.01	0.37 ± 0.02	0.39 ± 0.02
D_{10} (Gy)	6.12 ± 0.15	4.93 ± 0.16	4.60 ± 0.11*	4.70 ± 0.07*	4.57 ± 0.08**	3.84 ± 0.07**	3.82 ± 0.04**	3.92 ± 0.08**	4.06 ± 0.14**	4.21 ± 0.11**
D_{60} (Gy)	2.02 ± 0.12	1.68 ± 0.11	1.48 ± 0.18	1.55 ± 0.11*	1.50 ± 0.10**	1.08 ± 0.02**	1.10 ± 0.06**	1.16 ± 0.06**	1.09 ± 0.11**	1.14 ± 0.14**

The surviving parameters (α, β and α/β) were obtained from fitting the survival data with a linear–quadratic equation, and SF_2, D_{10} and D_{60} values were calculated using these parameters. [a] Mean ± standard error. *$0.01 < P < 0.05$, **$P < 0.01$, compared with the center of proton SOBP samples.

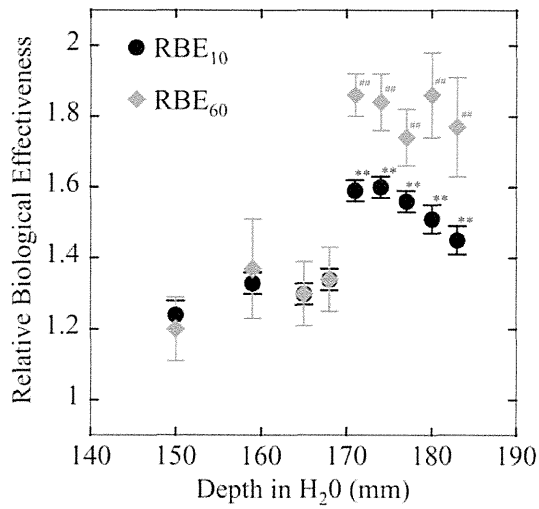

Fig. 3. Relative biological effectiveness (RBE) for HSG cells in a 190 MeV clinical proton beam with a 5-cm spread-out Bragg-peak (SOBP). RBE_{10} (closed circles) and RBE_{60} (closed diamonds) represent the RBE calculated using the biological equivalent dose, D_{10} and D_{60}, respectively. The symbols and bars are the mean and standard error (SE) obtained from at least three independent experiments. *$0.01 < P < 0.05$, **$P < 0.01$, compared with the center of the proton SOBP samples using RBE_{10}. #$0.01 < P < 0.05$, ##$P < 0.01$, compared with the center of the proton SOBP samples using RBE_{60}.

using the α and β values. RBE values of proton SOBP beams at 60% cell survival were defined as RBE_{60}, because the surviving fraction at 2 Gy SF_2 of X-rays is ~0.6. The RBE_{60} for HSG cells showed a maximum value of 1.56 at the distal end of the SOBP (Table 1). High-LET components could be effective on cells with small α and α/β values [28]. These high-LET components account for a large part of the total proton beams at the distal position in the SOBP, even after the decay of the SOBP when most of the beams lose energy. This could be the reason for the higher RBE values at 171–183 mmH_2O than at 150–168 mmH_2O positions.

Additionally, the more critical point in clinical settings is the shift of the distal edge of the biological dose compared with the isoeffective dose. According to the strong biological effect at the distal region of the proton SOBP, the biological depth–dose distribution may be extended to the direction of the proton beam prediction calculated by the generic RBE 1.1. In fact, unexpected normal tissue damage caused by the beam is rarely observed in the clinical field of proton therapy (personal communication with Dr Kanemoto, Proton Medical Research Center, Tsukuba University). According to a phenomenological model, one previous report showed that the distal edge of the biological dose was shifted from 1.1 to 2.2 mm for 80% physical dose points at 1–8 Gy [22]. Our results yielded 4.1 mm from the isoeffective dose at 2 Gy (Fig. 4). There are similarities between Wilkens's study

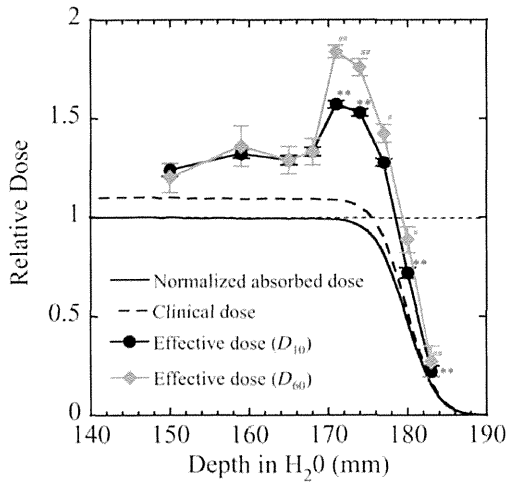

Fig. 4. Relative dose–depth distribution of the spread-out Bragg-peak (SOBP) of the 190 MeV proton beam. The biological dose was calculated as the relative biological effectiveness (RBE) × relative physical dose at each depth compared with the center. Effective dose (D_{10}) (closed circles) and effective dose (D_{60}) (closed diamonds) represents the biological dose calculated by the RBE_{10} and RBE_{60}, respectively. The symbols and bars are the mean and standard error (SE) obtained from at least three independent experiments. The solid line indicates the relative physical absorbed dose normalized with the center dose, and the dotted line indicates the clinical dose calculated from the generic proton RBE 1.1 × physical dose at each depth. $*0.01 < P < 0.05$, $**P < 0.01$, compared with the center of the proton SOBP samples using the effective dose (D_{10}). $^{\#}0.01 < P < 0.05$, $^{\#\#}P < 0.01$, compared with the center of the proton SOBP samples using the effective dose (D_{60}).

and our results. The distal shift could have been altered by the local energy distribution of the protons at the cells/tissues caused by the accelerated energy or the geometrical structure of the instruments upstream of the target. This study has certain limitations. We assessed the biological effects using one cell line (HSG cells) and one biological endpoint (cell survival). However, it is well known that the RBE values change depending on the kind of cells and endpoints [36]. Therefore, in any further study we will have to assess the biological effects using another cell line, other experimental animals and another biological technique (e.g. DNA repair, chromosomal aberration, mutation) [37–39].

There is also a problem regarding the use of the HSG cells. We chose HSG cells in this study because we have used HSG cells from the same cell line in experiments in particle beam facilities since the 1990s. Additionally, many laboratories (including ours) have used these cells in research and published many papers in international journals. However, it has been reported that the HSG cells used in this study were contaminated with HeLa cells [40, 41]. It will be necessary to consider the alternative cell line used for the particle beam facility experiments in the future.

CONCLUSION

In conclusion, the effective depth–dose distribution was not flat in the proton SOBP. RBE_{10} and RBE_{60} at the distal region of the SOBP showed a maximum of 1.5 and 1.7 at the 10% and 60% survival level, respectively. The uniform biological dose region at 90% of the prescribed dose extended to 3.6 and 4.1 mm, respectively. Distal-end regions of proton beams are characterized with high effectiveness, and the SOBP range may be extended by several mm in the direction of the beam. We suggest that it is desirable to take into consideration the biological dose distribution according to the depth in beam design and treatment planning, however, further research is crucial.

ACKNOWLEDGEMENTS

The authors are grateful to Ms Akiko Uzawa, Dr Ryoichi Hirayama, Ms Sachiko Koike, Dr Yuki Kase, Dr Chizuru Tsuruoka and Dr Ayae Kanemoto for experimental support in the cell survival assay and sample irradiation, and to Dr Takashi Ogino for managing the proton beam time for biological experiments.

FUNDING

This work was supported in part by the Special Coordination Funds of President for Research Projects with Heavy Ions at the National Institute of Radiological Sciences–Heavy-ion Medical Accelerator in Chiba (NIRS–HIMAC).

REFERENCES

1. Halperin E. Particle therapy and treatment of cancer. *Lancet Oncol* 2006;**7**:676–85.
2. Tuan J, Vischioni B, Fossati P *et al.* Initial clinical experience with scanned proton beams at the Italian National Center for Hadrontherapy (CNAO). *J Radiat Res* 2013;**54** Suppl 1: i31–42.
3. Srivastava A, Vischioni B, Fiore MR *et al.* Quality of life in patients with chordomas/chondrosarcomas during treatment with proton beam therapy. *J Radiat Res* 2013;**54** Suppl 1: i43–8.
4. Bert C, Engenhart-Cabillic R, Durante M. Particle therapy for noncancer diseases. *Med Phys* 2012;**39**:1716–27.
5. Clivio A, Kluge A, Cozzi L *et al.* Intensity modulated proton beam radiation for brachytherapy in patients with cervical carcinoma. *Int J Radiat Oncol Biol Phys* 2013;**87**:897–903.
6. PTCOG (Particle Therapy Coo-Operative Group). Particle therapy facilities in operation (incl. patient statistics). http ://ptcog.web.psi.ch/ptcentres.html (9 December 2013, date last accessed).
7. Ogino T. Clinical evidence of particle beam therapy (proton). *Int J Clin Oncol* 2012;**17**:79–84.
8. Matney J, Park PC, Bluett J *et al.* Effects of respiratory motion on passively scattered proton therapy versus intensity

modulated photon therapy for stage III lung cancer: are proton plans more sensitive to breathing motion? *Int J Radiat Oncol Biol Phys* 2013;**87**:576–82.
9. Góra J, Hopfgartner J, Kuess P *et al.* Is there room for combined modality treatments? Dosimetric comparison of boost strategies for advanced head and neck and prostate cancer. *J Radiat Res* 2013;**54** Suppl 1:i97–112.
10. Kase Y, Yamashita H, Fuji H *et al.* A treatment planning comparison of passive-scattering and intensity-modulated proton therapy for typical tumor sites. *J Radiat Res* 2012;**53**: 272–80.
11. Wambersie A, Menzel HG, Andreo P *et al.* Isoeffective dose: a concept for biological weighting of absorbed dose in proton and heavier-ion therapies. *Radiat Prot Dosim* 2011; **143**:481–6.
12. Gerweck LE, Kozin SV. Relative biological effectiveness of proton beams in clinical therapy. *Radiother Oncol* 1999;**50**:135–42.
13. Grégoire V, Pötter R, Wambersie A. General principles for prescribing, recording and reporting a therapeutic irradiation. *Radiother Oncol* 2004;**73** Suppl 2:S57–61.
14. Wambersie A, Hendry JH, Andreo P *et al.* The RBE issues in ion-beam therapy: conclusions of a joint IAEA/ICRU working group regarding quantities and units. *Radiat Prot Dosim* 2006;**122**:463–70.
15. Skarsgard LD. Radiobiology with heavy charged particles: a historical review. *Phys Med* 1998;**14** Suppl 1:1–19.
16. Paganetti H, Niemierko A, Ancukiewicz M *et al.* Relative biological effectiveness (RBE) values for proton beam therapy. *Int J Radiat Oncol Biol Phys* 2002;**53**:407–21.
17. Belli M, Bettega D, Calzolari P *et al.* Inactivation of human normal and tumour cells irradiated with low energy protons. *Int J Radiat Biol* 2000;**76**:831–9.
18. Bettega P, Calzolari P, Chauvel D. Radiobiological studies on the 65 MeV therapeutic proton beam at Nice using human tumour cells. *Int J Radiat Biol* 2000;**76**:1297–303.
19. Calugaru V, Nauraye C, Noël G *et al.* Radiobiological characterization of two therapeutic proton beams with different initial energy spectra used at the Institut Curie Proton Therapy Center in Orsay. *Int J Radiat Oncol Biol Phys* 2011;**81**:1136–43.
20. Britten RA, Nazaryan V, Davis LK *et al.* Variations in the RBE for cell killing along the depth-dose profile of a modulated proton therapy beam. *Radiat Res* 2013;**179**:21–8.
21. Paganetti H, Goitein M. Biophysical modelling of proton radiation effects based on amorphous track models. *Int J Radiat Biol* 2001;**77**:911–28.
22. Wilkens JJ, Oelfke U. A phenomenological model for the relative biological effectiveness in therapeutic proton beams. *Phys Med Biol* 2004;**49**:2811–25.
23. Kase Y, Yamashita W, Matsufuji N *et al.* Microdosimetric calculation of relative biological effectiveness for design of therapeutic proton beams. *J Radiat Res* 2013;**54**:485–93.
24. Nishio T, Kataoka S, Tachibana M *et al.* Development of a simple control system for uniform proton dose distribution in a dual-ring double scattering method. *Phys Med Biol* 2006;**51**:1249–60.
25. Baek H-J, Kim T-H, Shin D *et al.* Radiobiological characterization of proton beam at the National Cancer Center in Korea. *J Radiat Res* 2008;**49**:509–15.
26. Frese MC, Yu VK, Stewart RD *et al.* A mechanism-based approach to predict the relative biological effectiveness of protons and carbon ions in radiation therapy. *Int J Radiat Oncol Biol Phys* 2012;**83**:442–50.
27. Furusawa Y, Fukutsu K, Aoki M *et al.* Inactivation of aerobic and hypoxic cells from three different cell lines by accelerated (3)He-, (12)C- and (20)Ne-ion beams. *Radiat Res* 2000;**154**:485–96.
28. Ando K, Furusawa Y, Suzuki M *et al.* Relative biological effectiveness of the 235 MeV proton beams at the National Cancer Center Hospital East. *J Radiat Res* 2001;**42**:79–89.
29. Kase Y, Kanai T, Matsumoto Y *et al.* Microdosimetric measurements and estimation of human cell survival for heavy-ion beams. *Radiat Res* 2006;**166**:629–38.
30. Uzawa A, Ando K, Koike S *et al.* Comparison of biological effectiveness of carbon-ion beams in Japan and Germany. *Int J Radiat Oncol Biol Phys* 2009;**73**:1545–51.
31. Matsuura T, Egashira Y, Nishio T *et al.* Apparent absence of a proton beam dose rate effect and possible differences in RBE between Bragg peak and plateau. *Med Phys* 2010;**37**:5376–81.
32. Okamoto H, Kanai T, Kase Y *et al.* Relation between lineal energy distribution and relative biological effectiveness for photon beams according to the microdosimetric kinetic model. *J Radiat Res* 2011;**52**:75–81.
33. JSMP. Standard dosimetry of absorbed dose in external beam radiotherapy (Standard Dosimetry 01). Tsusho Sangyo Kenkyu Sha, Tokyo. 2002.
34. Wambersie A. RBE, reference RBE and clinical RBE: applications of these concepts in hadron therapy. *Strahlenther Onkol* 1999;**175** Suppl 2:39–43.
35. Suit H, Urie M. Proton beams in radiation therapy. *J Natl Cancer Inst* 1992;**84**:155–64.
36. Ando K, Kase Y. Biological characteristics of carbon-ion therapy. *Int J Radiat Biol* 2009;**85**:715–28.
37. Gueulette J, Bohm L, Slabbert JP *et al.* Proton relative biological effectiveness (RBE) for survival in mice after thoracic irradiation with fractionated doses. *Int J Radiat Oncol Biol Phys* 2000;**47**:1051–8.
38. Gueulette J, Blattmann H, Pedroni E *et al.* Relative biologic effectiveness determination in mouse intestine for scanning proton beam at Paul Scherrer Institute, Switzerland. Influence of motion. *Int J Radiat Oncol Biol Phys* 2005;**62**:838–45.
39. Kim SS, Choo DW, Shin D *et al.* *In vivo* radiobiological characterization of proton beam at the National Cancer Center in Korea: effect of the Chk2 mutation. *Int J Radiat Oncol Biol Phys* 2011;**79**:559–62.
40. International Cell Line Authentication Committee (ICLAC). *Database of Cross-Contaminated or Misidentified Cell Lines.* http://standards.atcc.org/kwspub/home/the_international_cell_line_authentication_committee-iclac_/Cross_Contaminations_v7_1.pdf (9 December 2013, date last accessed).
41. Capes-Davis A, Theodosopoulos G, Atkin I *et al.* Check your cultures! A list of cross-contaminated or misidentified cell lines. *Int J Cancer* 2010;**127**:1–8.